



# Vibrational properties of a mononuclear dysprosium containing singlemolecule magnet

Marco A. M. Tummeley<sup>1</sup> · Maren H. Hoock<sup>1</sup> · Konstantin Gröpl<sup>1</sup> · Rouven Pflieger<sup>2</sup> · Tim Hochdörffer<sup>1</sup> · Tim Hunsicker<sup>1</sup> · Juliusz A. Wolny<sup>1</sup> · Jiyong Zhao<sup>3</sup> · Barbara Lavina<sup>3</sup> · Michael Y. Hu<sup>3</sup> · Thomas Toellner<sup>3</sup> · Ercan E. Alp<sup>3</sup> · Hagen Kämmerer<sup>2</sup> · Christopher E. Anson<sup>2</sup> · Annie K. Powell<sup>2,4</sup> · Volker Schünemann<sup>1</sup>

Accepted: 18 January 2024  
© The Author(s) 2024

## Abstract

Dysprosium(III)-containing single-molecule magnets (SMMs) show blocking of the molecular magnetization and hysteresis effects in one molecule. They belong to the class of the best performing SMMs at present. Here, we present first results of <sup>161</sup>Dy-Nuclear Resonance Vibrational Spectroscopy (NRVS) experiments on the dysprosium(III) complex [Dy(H<sub>2</sub>dapp)(NO<sub>3</sub>)<sub>2</sub>](NO<sub>3</sub>) with H<sub>2</sub>dapp being 2,6-bis((E)-1-(2-(pyridine-2-yl)hydrazineylidene)ethyl)pyridine. For the <sup>161</sup>Dy-NRVS experiments a compact novel He flow cryostat was used at the Advanced Photon Source, Argonne National Laboratories, which enables low temperature NRVS experiments in helium vapour circumventing the often-observed difference between sensor read and “real” sample temperature in mostly used LHe and/or closed cycle cryostats with the NRVS sample being in vacuum. To explore the vibrational modes of the molecule simulations based on first density functional theory (DFT) calculations are presented.

**Keywords** Dysprosium complexes · Nuclear forward scattering · Nuclear inelastic scattering · Nuclear resonance vibrational spectroscopy · Density functional theory · Cryostat

---

✉ Volker Schünemann  
schuene@rptu.de

<sup>1</sup> Department of Physics, RPTU Kaiserslautern-Landau, Erwin-Schrödinger-Str. 46, 67663 Kaiserslautern, Germany

<sup>2</sup> Institute of Inorganic Chemistry, Karlsruhe Institute of Technology, 76131 Karlsruhe, Germany

<sup>3</sup> Advanced Photon Source, Argonne National Laboratory, 60439 Argonne, IL, USA

<sup>4</sup> Institute of Nanotechnology, Karlsruhe Institute of Technology, 76131 Karlsruhe, Germany

## 1 Introduction

Single-molecule magnets (SMMs) exhibit long magnetization relaxation times and hysteresis effects at low temperatures. The possibility of integrating specific functions, like switching states with light or electric fields would make SMMs a suitable contender against thin film magnetic materials in future spintronics applications [1]. Among the best performing SMMs are Dy-containing compounds showing high blocking temperatures and long relaxation times of the magnetization reversal [2]. A significant obstacle to forcing the SMM system to relax over the barrier is that Quantum Tunnelling of the Magnetisation (QTM) provides an easy under-barrier pathway. It has recently been pointed out that coupling between relaxation mechanisms and molecular vibrations including phonon modes promotes this QTM [3–10].

This motivated us to perform time-domain  $^{161}\text{Dy}$ -Mössbauer spectroscopy (Nuclear Forward Scattering (NFS)) [11] and  $^{161}\text{Dy}$ -Nuclear Resonance Vibrational Spectroscopy (NRVS) on a mononuclear Dy containing SMM [12]. Here, we present  $^{161}\text{Dy}$ -NRVS on a further mononuclear dysprosium(III) complex **1**  $[\text{Dy}(\text{H}_2\text{dapp})(\text{NO}_3)_2](\text{NO}_3)$  with pentadentate ligand  $\text{H}_2\text{dapp}$  being 2,6-bis((E)-1-(2-(pyridin-2-yl)-hydrazineylidene)ethyl)pyridine [13]. A structural view of this complex is shown in Fig. 1. The material exhibits zero field quantum tunnelling of its magnetisation as shown by AC susceptibility measurements, but it displays a maximum in the out of phase AC susceptibility when applying a field of 3000 Oe. In this way frequency dependent out of phase measurements were detectable between 0.1 and 1 Hz up to 5 K, which is characteristic for SMM behaviour [13].

To explore the vibrational properties of complex **1** first simulations based on quantum chemical density functional theory (DFT) calculations of a single molecule model are presented to identify those molecular vibrations which might influence its SMM properties.

## 2 Materials and methods

The mononuclear complex **1** was synthesized according to the description given in ref. [13]. Isotope labelling was achieved by using 91% enriched  $^{161}\text{Dy}_2\text{O}_3$  for the synthesis.

$^{161}\text{Dy}$ -NRVS was performed at the beamline 3-ID-B at the Advanced Photon Source (APS) at Argonne National Laboratory. The synchrotron was run in the standard operating mode (top-up) with a bunch separation of 153 ns. A monochromator setup for the  $^{161}\text{Dy}$  nuclear resonance (25.651 keV) was used as described in [14, 15]. To achieve maximum NRVS count rate at lowest possible sample temperature, the experiments were carried out by utilization of a compact liquid helium flow cryostat. The cryostat manufactured by Janis Ltd. is equipped with a diamond window located at the bottom of a variable temperature inset (VTI). The sample was mounted on top of a sample holder (Fig. 2a, b) which was positioned upside down on the sample rod of the cryostat (Fig. 2c, d). In this way the sample could be positioned 1 mm above the diamond window of the VTI (Fig. 2e). The sample holder was 3D printed with an Ultimaker S5 3D using an optically transparent copolyester (Ultimaker CPE<sup>+</sup>-Filament). The cryostat has two axial windows made out of Kapton© which transmit the monochromatized synchrotron radiation in order to excite the sample and allow measuring NFS data and instrumental function. Optional, together with the NIS sample a second sample for NFS can be mounted into the sample holder (Fig. 2f). Since the

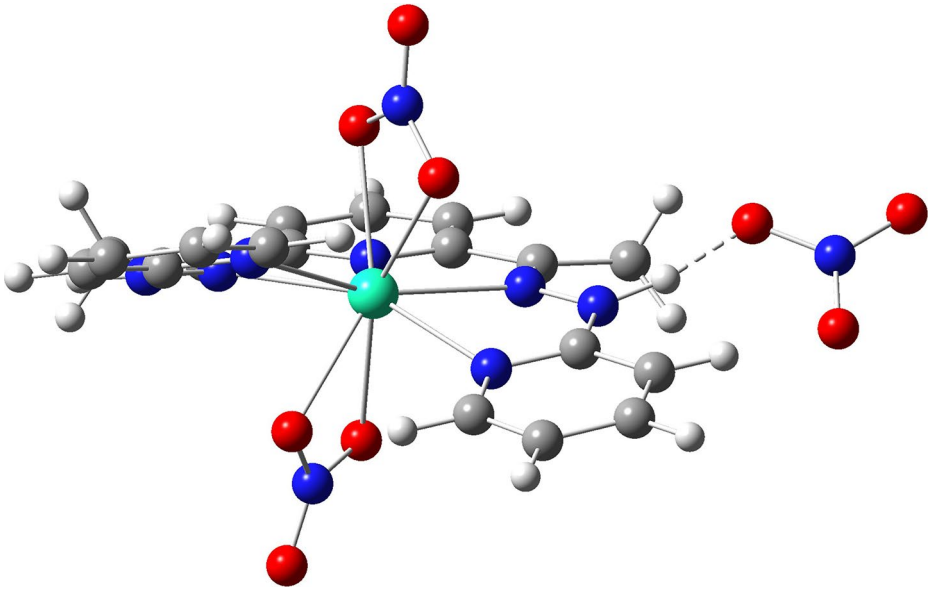


**Fig. 1** Structural view of the mononuclear Dy complex **1** investigated in this study. There are two axial  $\text{NO}_3^-$  ions coordinating to the Dy ion and one  $\text{NO}_3^-$  acting as counter ion which is not coordinated to the Dy ion (right). The atoms are color coded as follows: Dysprosium atom turquoise, nitrogen atoms blue, carbon atoms dark grey, oxygen atoms red and hydrogens white On the PDF version, place Figs. 1, 2, and 5 at the top of the page as per journal special instruction

sample holder is not in vacuum but in an He atmosphere, both samples have the same temperature. The base temperature of the cryostat can be as low as 1.6 K, the NRVS measurements presented here have been done at 10 K. Temperature control was achieved using a LS 335 temperature controller from Lake Shore Cryotronics, Inc., in combination with a Cernox sensor placed on the sample rod above the sample mount. The incoherently scattered radiation (NRVS signal) passes the diamond window and successively a room temperature window made out of beryllium which is mounted at the top of a reentrant bore tube of the cryostat. The NRVS scans were recorded with an Avalanche Photo Diodes (APD) placed inside the reentrant bore tube in a distance of  $\sim 8$  mm from the sample in closest distance in order to maximize signal. It should be mentioned that sample loading into the cryostat was performed within seconds by precooling the sample rod in  $\text{LN}_2$  and inserting it into the VTI with the He flow being shut down. After insertion the sample temperature did not raise above 77 K. Thus, this procedure can also be applied in case of measuring delicate reactive air sensitive samples by NRVS.

The energy of the incoming synchrotron beam, focused to 20  $\mu\text{m}$ , was varied from  $-20$  meV to 70 meV around the nuclear resonance transition energy of 25.651 keV. The herein presented NRVS data result from a sum of 13 scans with each scan being recorded with a step size of 0.25 meV and a data acquisition time of 3 s/point. The energy resolution was  $0.61 \pm 0.06$  meV ( $4.9 \pm 0.5$   $\text{cm}^{-1}$ ). The  $^{161}\text{Dy}$  phonon density of states (pDOS) was determined with the software PHOENIX [16], taking the resonance energy of 25.651 keV and recoil energy of 2.195 meV into account [17]. The data evaluation procedure removes the

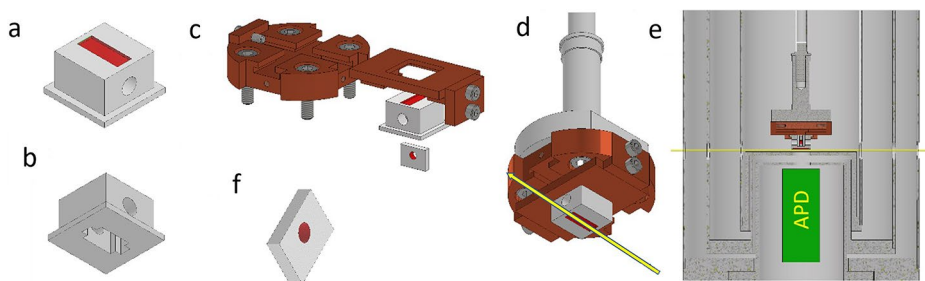


**Fig. 2** 3D printed sample holder with a NRVS sample slot of  $8.4 \text{ mm} \times 3.0 \text{ mm} \times 0.5 \text{ mm}$  marked in red (a). The powder sample was covered with adhesive Kapton<sup>®</sup> tape. Into the back of the sample holder (b) an NFS sample holder can be slid in (c) and (f). The NFS sample slot has a diameter of 1.5 mm and a depth of 1.5 mm. The synchrotron beam touches the sample as shown in (d). Inside the VTI of the cryostat the sample is in He vapour and mounted app. 1 mm above the bottom of the VTI which has a diamond window (e). The APD detector is mounted as closed as possible to the room temperature Be window of the cryostat within a reentrant bore tube

elastic contribution from the NRVS data and separates the single-phonon absorption from multiphonon contributions based on a harmonic lattice model [16].

DFT calculations were performed with the Gaussian16 software package [18]. The structures were optimized with the functional B3LYP and the CEP-31G basis set based on the structural model shown in Fig. 1. The partial density of states (pDOS) of the Dy-atoms were extracted out of the calculated frequencies with the software nisspec2 [19].

### 3 Results and discussion

The experimental NRVS data of the mononuclear  $^{161}\text{Dy}$  complex **1** is shown in Fig. 3. The temperature within the VTI was 10 K and was controlled with the temperature controller. Due to the low temperature, there are no anti-Stokes bands visible at wavenumbers higher than  $30 \text{ cm}^{-1}$  below the nuclear resonance energy. To determine the temperature of the sample itself experimentally we have used the intensity ratio for phonon creation  $I(E)$  and annihilation  $I(-E)$  for three Stokes and anti-Stokes bands as indicated by the blue arrows in Fig. 3. With  $T(E) = (E/k_B) / (\ln[I(E)/I(-E)])$  we obtain  $T = 10 \pm 0.2 \text{ K}$  in excellent agreement with the set temperature.

The experimental pDOS of complex **1** obtained from the NRVS data shown in Fig. 3 is displayed in Fig. 4a. The pDOS shows a very strong structured band below  $50 \text{ cm}^{-1}$  and a group of bands between 135 and  $180 \text{ cm}^{-1}$  with medium intensity. From 180 up to  $216 \text{ cm}^{-1}$  again an intensive broad spectral feature with at least three distinct bands occurring at 186, 202 and  $208 \text{ cm}^{-1}$  is observed. This is followed by a further broad band with multiple peaks between 218 and  $275 \text{ cm}^{-1}$ . At higher wavenumbers the identification of individual bands is hampered by spectral noise. The analysis of the experimental pDOS leads to a Lamb-Möbbaauer factor  $f_{LM}(T=0 \text{ K}) = 0.76 \pm 0.01$  and a mean force constant of  $D = 211 \pm 25 \text{ Nm}^{-1}$ . The so observed mean force constant agrees well with that of one of the best performing mononuclear SMMs, an 8O coordinated Dy phosphine complex ( $D = 212 \pm 25 \text{ Nm}^{-1}$ ; [12]) which shows blocked dc magnetization up to 20 K. The value of the Lamb-Möbbaauer factor of the latter is the same as that of complex **1**.

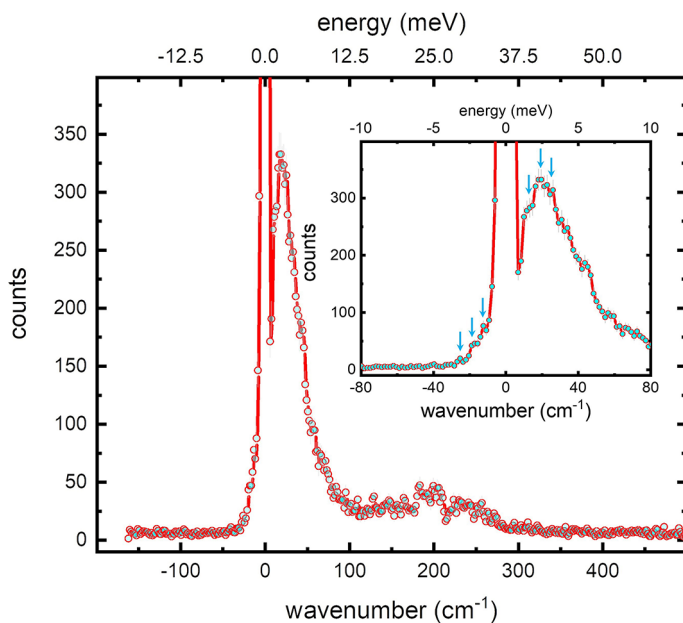


**Fig. 3** Experimental NRVS data of the mononuclear  $^{161}\text{Dy}$  complex **1** as a function of energy shift  $E$  from the  $^{161}\text{Dy}$  nuclear resonance. The elastic peak caused by the resonant photons with 25.651 keV occurs at  $E=0 \text{ cm}^{-1}$  and is out of scale. The inset shows the spectral region from  $-80$  to  $+80 \text{ cm}^{-1}$  with the blue arrows depicting the positions of the three  $I(E)$  values used for the determination of the sample temperature ( $T=10.2\pm 0.6 \text{ K}$ ) as explained in the text

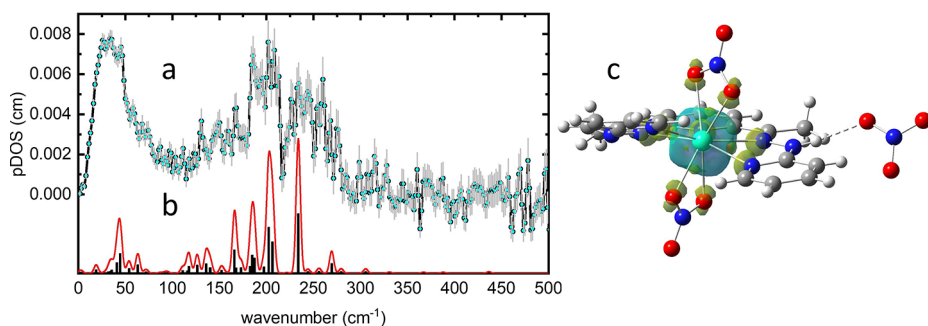


**Fig. 4** Experimental pDOS of the mononuclear  $^{161}\text{Dy}$  complex **1** obtained from NRVS at  $10 \text{ K}$  (a) and simulated pDOS obtained via DFT calculations as described in the text (b). The complex shows localization of unpaired spin-up electron density at the Dy (turquoise) but also unpaired spin-down electron density (dark yellow) at the coordinating four N and O atoms (c)

Figure 4b shows a DFT simulated pDOS obtained after energy minimization of the structural model displayed in Fig. 1 including the  $\text{NO}_3^-$  counter ion and subsequent normal mode calculation. The so obtained positions of the vibrational modes having  $^{161}\text{Dy}$  movement are shown in black bars with their intensity being proportional to the mean square displacement of the  $^{161}\text{Dy}$  atom within each mode. The resulting pDOS (red line) has been calculated as a

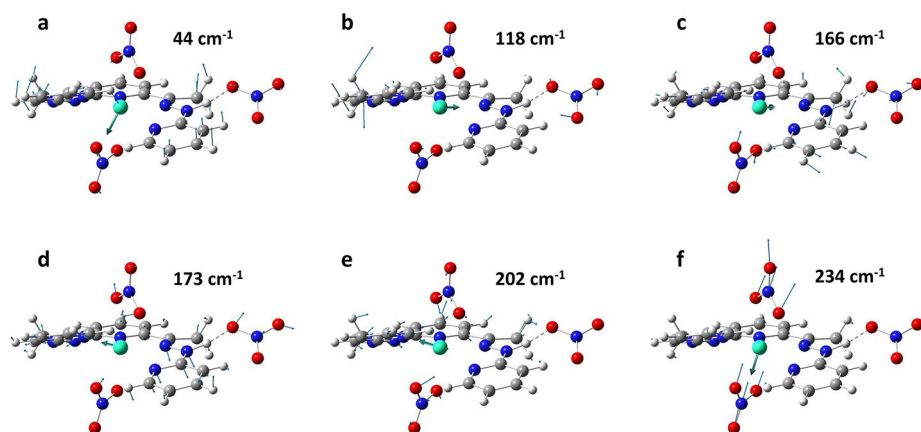


**Fig. 5** Selected vibrational modes of complex **1** with wavenumbers indicated as discussed in the text obtained by DFT calculations. The displacement vectors of the dysprosium and oxygen atoms are color coded the same as the corresponding atoms

sum of the individual Gaussian mode profiles with the full width at half maximum given by the experimental resolution of  $4.9\text{ cm}^{-1}$ . In the following we discuss the six most prominent vibrational modes (Fig. 5 and corresponding videos in SI).

The mode calculated to occur at  $44\text{ cm}^{-1}$  (Fig. 5a) shows a movement of the whole molecule accompanied by a butterfly-like motion of the  $\text{H}_2\text{dapp}$  ligand. The two axial  $\text{NO}_3^-$  and the central Dy are moving together in a direction perpendicular to the  $\text{H}_2\text{dapp}$  ligand (see also video\_44). At  $118\text{ cm}^{-1}$  there is a mode involving the movement of the whole molecule with a high-amplitude of rotation of the methyl residues of the  $\text{H}_2\text{dapp}$  ligand (Fig. 5b, video\_118). The rest of the molecule reveals a rocking motion of the aromatic rings coupled with rocking of the nitrate anions.

At  $166\text{ cm}^{-1}$  (Fig. 5c, video\_166) the  $\text{H}_2\text{dapp}$  ligand displays a motion like that at  $118\text{ cm}^{-1}$  with a higher amplitude of the ring rocking and a different direction of Dy-atom movement. The similar holds for the vibration predicted at  $173\text{ cm}^{-1}$  (Fig. 5d, video\_173). The mode reveals a somewhat higher amplitude of the movement of the terminal  $\text{H}_2\text{dapp}$  pyridine rings. In addition, stretching of the Dy and the nitrate oxygen is visible. At  $202\text{ cm}^{-1}$  (Fig. 5e, video\_202) an in-plane motion of the Dy is observed revealing Dy-N bending and stretching. Like in the mode at  $173\text{ cm}^{-1}$  the  $\text{NO}_3^-$  ligand rotates and thus, the mode has Dy-O stretching character. There is also  $\text{H}_2\text{dapp}$  ligand bending. The stretching mode calculated at  $234\text{ cm}^{-1}$  (Fig. 5f, video\_234) reveals a predominant Dy-nitrate axial stretching movement.

Comparison of experimental and simulated pDOS region below  $70\text{ cm}^{-1}$  shows that there is considerable disagreement. Obviously long range low energy acoustic phonons are excited in the solid sample which cannot be calculated by DFT calculations of a single molecule as been done in this study. We tentatively assign the broad experimental band structure between  $186$  and  $208\text{ cm}^{-1}$  to modes with considerable Dy-N stretching character (Fig. 5c–e) and those higher than  $218\text{ cm}^{-1}$  to modes with Dy-nitrate stretching character like e.g. displayed in Fig. 5f. The fact that we observe relative broad experimental band in the pDOS may be caused by significant interaction of the nitrate counterions in between the

single unit cells. We are currently investigating this issue by performing DFT calculations on structural models having up to ten unit cells.

In addition to the vibrational properties DFT calculations give insight into electronic properties. Therefore, we also have calculated the spin-up and spin-down electron densities of complex **1** as shown in Fig. 4c. There is localized dominating positive spin-up electron density as expected for 4f dysprosium(III) systems. Similar to previous results obtained for the Dy phosphine SMM [12] there is also spin density at the coordinating ligand atoms of complex **1**. The DFT calculations presented here show that there is negative spin density at the four equatorial nitrogen ligands and also at the oxygen atoms of the two axial coordinating  $\text{NO}_3^-$  ions. This might contribute to the reported dependence of the SMM properties on the nature of the counter ion of this kind of Dy complexes [13].

## 4 Conclusions

Using a novel continuous flow He cryostat and a corresponding 3D printed sample holder design  $^{161}\text{Dy}$ -NRVS experiments have delivered the pDOS of a dysprosium(III) containing SMM. Quantum chemical DFT calculations based on a structural model of the SMM  $[\text{Dy}(\text{H}_2\text{dapp})(\text{NO}_3)_2]^+$  have been performed under inclusion of the  $\text{NO}_3^-$  counter ion in order to simulate the experimental pDOS. Given the special role of the counter ions in the SMM performance of dysprosium(III) complexes with  $\text{H}_2\text{dapp}$  ligands DFT calculations on multiple unit cells of the complex are foreseen. This will improve the agreement between experimental and simulated pDOS and might also give insight into those phonons which may be mediated by the  $\text{NO}_3^-$  ions and lead to phonon induced quantum tunnelling of the magnetization in complex **1** in zero applied fields.

**Supplementary Information** The online version contains supplementary material available at <https://doi.org/10.1007/s10751-024-01857-6>.

**Acknowledgements** This research used resources of the Advanced Photon Source (APS), a U.S. Department of Energy (DOE) Office of Science User Facility operated for the U.S. DOE Office of Science by Argonne National Laboratory (ANL) under Contract No. DE-AC02-06CH11357. The data were collected at 3-ID beamline. V.S. and A.K.P. acknowledge the support by the Deutsche Forschungsgemeinschaft (DFG) through CRC/TRR88, “Cooperative Effects in Homo- and Hetero-Metallic Complexes(3MET)”. V.S. also acknowledges support through the CRC/TRR173 “Spin+X” and by the German Ministry of Research (BMBF) under 05K22UK2.

**Author contributions** M.A.M.T. and V.S. wrote the main manuscript text. M.H.H., K.G., T. Ho., J.Z., B.L., M.Y.H., T.T., V.S. and E.E.A. performed the NIS experiments at the beamline. M.A.M.T. and M.H.H. performed data analysis. J.A.W. performed DFT calculations. V.S. wrote application for beamtime. T. Hu. designed and built the sample holder. R.P., H.K., C.E.A. and A.K.P. provided the sample. All authors reviewed the manuscript.

**Funding** Deutsche Forschungsgemeinschaft (DFG): CRC/TRR88, “3MET”, Projects A03 and A04; CRC/TRR173 “Spin+X”, Project A04. German Federal Ministry of Education and Research (BMBF): Project 05K22UK2. U.S. Department of Energy (DOE) Office of Science: Contract No. DE-AC02-06CH11357. Open Access funding enabled and organized by Projekt DEAL.

**Data availability** Any data is available on request to either the first or the communicating author.

## Declarations

**Ethical approval** Not applicable, no human and/ or animal studies.

**Competing interests** The authors declare no competing interests.

**Open Access** This article is licensed under a Creative Commons Attribution 4.0 International License, which permits use, sharing, adaptation, distribution and reproduction in any medium or format, as long as you give appropriate credit to the original author(s) and the source, provide a link to the Creative Commons licence, and indicate if changes were made. The images or other third party material in this article are included in the article's Creative Commons licence, unless indicated otherwise in a credit line to the material. If material is not included in the article's Creative Commons licence and your intended use is not permitted by statutory regulation or exceeds the permitted use, you will need to obtain permission directly from the copyright holder. To view a copy of this licence, visit <http://creativecommons.org/licenses/by/4.0/>.

## References

1. Liu, J.-L., Chen, Y.-C., Tong, M.-L.: Symmetry strategies for high performance lanthanide-based single-molecule magnets. *Chem. Soc. Rev.* **47**, 2431–2453 (2018). <https://doi.org/10.1039/C7CS00266A>
2. Bogani, L., Wernsdorfer, W.: Molecular spintronics using single-molecule magnets. *Nat. Mater.* **7**, 179–186 (2008). <https://doi.org/10.1038/nmat2133>
3. Escalera-Moreno, L., Suaud, N., Gaita-Arino, A., Coronado, E.: Determining Key Local vibrations in the relaxation of Molecular Spin qubits and single-molecule magnets. *Phys. Chem. Lett.* **8**, 1695–1700 (2017). <https://doi.org/10.1021/acs.jpcclett.7b00479>
4. Pedersen, K.S., Dreiser, J., Weihe, H., Sibille, R., Johannesen, H.V., Sorensen, M.A., Nielsen, B.E., Sigrist, M., Mutka, H., Rols, S., Bendix, J., Piligkos, S.: Design of single-molecule magnets: Insufficiency of the anisotropy barrier as the sole criterion. *Inorg. Chem.* **54**, 7600–7606 (2015). <https://doi.org/10.1021/acs.inorgchem.5b01209>
5. Escalera-Moreno, L., Baldov, J.J., Gaita-AriCo, A., Coronado, E.: Spin states, vibrations and spin relaxation in molecular nanomagnets and spin qubits: a critical perspective. *Chem. Sci.* **9**, 3265–3275 (2018). <https://doi.org/10.1039/C7SC05464E>
6. Zhang, P., Zhang, L., Tang, J.: Lanthanide single molecule magnets: Progress and perspective. *Dalton Trans.* **44**, 3923–3929 (2015). <https://doi.org/10.1039/C4DT03329A>
7. Lunghi, A., Totti, F., Sanvito, S., Sessoli, R.: Intra-molecular origin of the spin-phonon coupling in slow-relaxing molecular magnets. *Chem. Sci.* **8**, 6051–6059 (2017). <https://doi.org/10.1039/C7SC02832F>
8. a) Atzori, M., Tesi, L., Benci, S., Lunghi, A., Righini, R., Taschin, A., Torre, R., Sorace, L., Sessoli, R.: Spin Dynamics and Low Energy Vibrations: Insights from Vanadyl-Based Potential Molecular Qubits. *J. Am. Chem. Soc.* **139** 4338–4341, Blagg, R.J., Ungur, L., Tuna, F., Speak, J., Comar, P., Collison, D., Wernsdorfer, W., McInnes, E.J.L., Chibotaru, L.F., Winpenny, R.E.P.: Magnetic relaxation pathways in lanthanide single-molecule magnets. *Nat. Chem.* **5**, 673–678 (2013). <https://doi.org/10.1038/nchem.1707> c), Goodwin, C.A.P., Ortu, F., Reta, D., Chilton, N.F.: Mills, D.P.: Molecular magnetic hysteresis at 60 kelvin in dysprosocenium. *Nature* **548**, 439–442 (2017). <https://doi.org/10.1038/nature23447> (2017)
9. Rechkemmer, Y., Breitgoff, F.D., van der Meer, M., Atanasov, M., Hakl, M., Orlita, M., Neugebauer, P., Neese, F., Sarkar, B., van Slageren, J.: A four-coordinate cobalt(II) single-ion magnet with coercivity and a very high energy barrier *Nat. Commun.* **7**, 10467 (2016). <https://doi.org/10.1038/ncomms10467>
10. Moseley, D.H., Stavretis, S.E., Thirunavukkuarasu, K., Ozerov, M., Cheng, Y., Daemen, L.L., Ludwig, J., Lu, Z., Smirnov, D., Brown, C.M., Pandey, A., Ramirez-Cuesta, A.J., Lamb, A.C., Atanasov, M., Bill, E., Neese, F., Xue, Z.-L.: Spin-phonon couplings in transition metal complexes with slow magnetic relaxation. *Nat. Commun.* **9**, 2572 (2018). <https://doi.org/10.1038/s41467-018-04896-0>
11. Scherthan, L., Schmidt, S.F.M., Auerbach, H., Hochdörffer, T., Wolny, J.A., Bi, W., Zhao, J., Hu, M.Y., Toellner, T., Alp, E.E., Brown, D.E., Anson, C.E., Powell, A.K., Schünemann, V.: 161 Dy Time-Domain Synchrotron Mössbauer Spectroscopy for investigating single-molecule magnets incorporating Dy Ions. *Angew Chem. Int. Ed. Engl.* **58**, 3444–3449 (2019). <https://doi.org/10.1002/anie.201810505>

12. Scherthan, L., Pfleger, R.F., Auerbach, H., Hochdörffer, T., Wolny, J.A., Bi, W., Zhao, J., Hu, M.Y., Alp, E.E., Anson, C.E., Diller, R., Powell, A.K., Schünemann, V.: Exploring the vibrational side of Spin-Phonon Coupling in single-molecule magnets via 161 Dy Nuclear Resonance Vibrational Spectroscopy. *Angew Chem. Int. Ed. Engl.* **59**, 8818–8822 (2020). <https://doi.org/10.1002/anie.201914728>
13. Pfleger, R.F., Schlittenhardt, S., Merkel, M.P., Ruben, M., Fink, K., Anson, C.E., Bendix, J., Powell, A.K.: Terminal Ligand and packing effects on slow relaxation in an Isostructural Set of Dy(H<sub>2</sub>dpp)X<sub>2</sub>+single molecule Magnets\*. *Chemistry*. **27**(155086–15094) (2021). <https://doi.org/10.1002/chem.202102918>
14. Brown, D.E., Toellner, T.S., Sturhahn, W., Alp, E.E., Hu, M., Kruk, R., Rogacki, K., Canfield, P.C.: Partial Phonon density of States of Dysprosium and its compounds measured using Inelastic Nuclear Resonance Scattering. *Hyperfine Interact.* **153**, 17–24 (2004). <https://doi.org/10.1023/B:HYPE.0000024710.30209.72>
15. Toellner, T.S., Hu, M.Y., Bortel, G., Sturhahn, W., Shu, D.: Four-reflection nested mev-monochromators for 20–30 keV synchrotron radiation. *Nucl. Instr Meth Phys. Res. A.* **557**, 670–675 (2006). <https://doi.org/10.1016/j.nima.2005.11.114>
16. Sturhahn, W.: CONUSS and PHOENIX: Evaluation of nuclear resonant scattering data. *Hyperfine Interact.* **125**, 149–172 (2000). <https://doi.org/10.1023/A:1012681503686>
17. Shvyd'ko, Y.V., Lucht, M., Gerdau, E., Lerche, M., Alp, E.E., Sturhahn, W., Sutter, J., Toellner, T.S.: Measuring wavelengths and lattice constants with the Mössbauer wavelength standard. *J. Synchrotron Rad.* **9**, 17–23 (2002). <https://doi.org/10.1107/S0909049501019203>
18. Frisch, M.J., Trucks, G.W., Schlegel, H.B., Scuseria, G.E., Robb, M.A., Cheeseman, J.R., Scalmani, G., Barone, V., Petersson, G.A., Nakatsuji, H., Li, X., Caricato, M., Marenich, A.V., Bloino, J., Janesko, B.G., Gomperts, R., Mennucci, B., Hratchian, H.P., Ortiz, J.V., Izmaylov, A.F., Sonnenberg, J.L., Williams-Young, D., Ding, F., Lipparini, F., Egidi, F., Goings, J., Peng, B., Petrone, A., Henderson, T., Ranasinghe, D., Zakrzewski, V.G., Gao, J., Rega, N., Zheng, G., Liang, W., Hada, M., Ehara, M., Toyota, K., Fukuda, R., Hasegawa, J., Ishida, M., Nakajima, T., Honda, Y., Kitao, O., Nakai, H., Vreven, T., Throssell, K., Peralta, M. Jr., Ogliaro, J.E., Bearpark, F., Heyd, M.J., Brothers, J.J., Kudin, E.N., Staroverov, K.N., Keith, V.N., Kobayashi, T.A., Normand, R., Raghavachari, J., Rendell, K., Burant, A.P., Iyengar, J.C., Tomasi, S.S., Cossi, J., Millam, M., Klene, J.M., Adamo, M., Cammi, C., Ochterski, R., Martin, J.W., Morokuma, R.L., K., Farkas, O., Foresman, J.B., Fox, D.J.: *Gaussian 16 Rev. C.01*. Gaussian Inc. Wallingford CT (2016)
19. Paulsen, H., Winkler, H., Trautwein, A.X., Grünsteudel, H., Rusanov, V., Toftlund, H.: Measurement and simulation of nuclear inelastic-scattering spectra of molecular crystals. *Phys. Rev. B.* **59**, 975–984 (1999). <https://doi.org/10.1103/PhysRevB.59.975>